A Wideband CMOS NMR Spectrometer for Multinuclear Molecular Fingerprinting

Aoyang Zhang, Daniel Krüger, Behdad Aghelnejad, Guang Yang, Henry Hinton, Yi-Qiao Song, and Donhee Ham

Harvard University, Cambridge, MA, USA; Email: aoyang@seas.harvard.edu; donhee@seas.harvard.edu

Abstract

We report a wideband (1-100 MHz) CMOS spectrometer capable of multinuclear nuclear magnetic resonance (NMR) spectroscopy and demonstrate it by performing ^{1}H, ^{19}F, and ^{2}H NMR spectroscopy with high spectral resolution down to 0.07 ppm. This is made possible by developing a wideband, digitally assisted CMOS RF transceiver, where a delay-locked loop (DLL) with a broad locking range is the most critical functional block for enabling operation across the full experimental bandwidth. This portable multinuclear NMR system can enhance the capability of online molecular fingerprinting.

Keywords: CMOS, integrated circuit, RF transceiver, NMR.

Introduction

The past 15 years have seen the emergence and improvement of small nuclear magnetic resonance (NMR) systems comprising integrated CMOS RF transceivers and permanent magnets [1-5]. They can potentially make the analytical power of NMR broadly available beyond dedicated facilities, with on-site molecular fingerprinting being a particularly useful application. These small systems have so far been largely focused on ^{1}H NMR using narrow-band RF transceivers. Here we report a small NMR system with a wideband (1 ~ 100 MHz) CMOS RF transceiver to perform NMR not only on ^{1}H protons but also on other NMR-active nuclei (*e.g.*, those from ^{19}F and ^{2}H), thus expanding the molecular fingerprinting capability.

Fig. 1 illustrates our small NMR system. Its two major components are the wideband CMOS RF transceiver chip and a 0.51-T permanent Halbach magnet. A sample tube (inner diameter: 0.4 mm) wound with an RF coil is placed in the magnet bore, and the RF coil is connected to the CMOS RF transceiver. The sample tube can be rotated by a DC motor for motional averaging, which together with shimming coils (not to be confused with the RF coil) enhances the spectral resolution down to 0.07 ppm, with which fine NMR spectra such as *J*-coupling can be resolved. We present the design of the wideband CMOS RF transceiver and the measurement results below.

Wideband CMOS RF Transceiver

The architecture of the CMOS RF transceiver is shown in Fig. 2. In the heterodyning RF receiver (RX), the voltage signal across the RF coil induced by nuclear spin precessions, is amplified first by a differential low-noise amplifier, then by a variable gain amplifier and is subsequently down-converted by quadrature mixers. The down-converted quadrature signals are low-pass filtered with additional amplification. The front-end of the RF transmitter (TX) of Fig. 2 is the digital power amplifier (PA), whose detailed schematic is shown in Fig. 3. To increase the power efficiency and output voltage swing, we designed a self-biasing, 3-stack class-D digital PA. To minimize voltage stress, deep *n*-well transistors are used in the PA. The deep *n*-well connects to $3V_{DD}$ through a large resistor so that the parasitic *pn* junction is not forward biased and also so that parasitic loss is minimized. The measured PA peak output waveform in Fig. 3 shows a single-ended, 9 V peak-to-peak swing and a maximum drain efficiency of 49% for a 25-Ω load.

The chip also contains a wideband delay-locked loop (DLL) as a multi-phase generator and an arbitrary pulse sequencer with an on-chip 64 × 89-bit memory bank. These two functional blocks together control the amplitude and phase of the digital PA to perform versatile manipulation of nuclear spins. For example, the DLL generates 32 uniform phases and chooses any one of them for the excitation RF signal. Its 2-bit delay cells with switched capacitors are utilized to tune the delay. This leads to a large locking range for the DLL, which enables the wideband operation of the CMOS RF transceiver. For the DLL, an additional duty-cycle correction loop is used to maintain a 50% duty cycle, avoiding output power degradation. Overall, the TX assisted by the DLL and arbitrary pulse sequencer can produce a suite of RF excitation signals by using 14 amplitudes, 32 phases, and various time delays. The parameters for RF excitation signals are stored in the on-chip memory bank. Finally, the chip also incorporates three 8-bit digital to analog converters (DACs) to control the shimming coils.

Measurements

The RF transceiver is fabricated in a 0.18 μm CMOS technology (Fig. 5). Fig. 4 shows its measurements. The RX input referred noise is < 1.2 nV/√Hz over the 1 - 100 MHz bandwidth, with a minimum of 0.67 nV/√Hz at 21 MHz, the ^{1}H NMR frequency for the 0.51-T static magnetic field. The maximum RX gain is >100 dB over the 1 - 100 MHz bandwidth, with a maximum gain of 112 dB at 1 MHz. The RX gain is tunable from 30 to 110 dB at 21 MHz. The measured 32 phases of the DLL show less than ±0.6-degree phase errors at 21 MHz, which is sufficient for high resolution spectroscopy. The measured phase noise of the wideband DLL achieves an integrated 28.2/9.26-ps RMS jitter at 20/40 MHz, respectively (Fig. 4). The PA delivers a maximum of 860 mA peak output current at 21 MHz, with a tunable range from 63 mA to 860 mA. In addition to the room temperature measurements above, the RX gain varies less than 4 dB between 25 and 125 °C, where the PA output current degrades less than 1 dB, due to the temperature resilient design of our transceiver.

Fig. 6, 7, and 8 show NMR experiments performed with our system. The ^{1}H free-induction decays (FIDs) measured with the 0.51-T static magnetic field (^{1}H NMR frequency ~ 21.8 MHz) and the 0.3-T static magnetic field (^{1}H NMR frequency ~ 12.8 MHz) indicate the wideband capability of our system (Fig. 6). The measurements of ^{1}H spin-spin relaxation time T_2 at different temperatures (Fig. 7) confirm the relaxometry capability. Fig. 8 shows the measured ^{1}H, ^{19}F, and ^{2}H NMR spectra (21.8 MHz, 20.5 MHz, and 3.3 MHz for 0.51-T static magnetic field) in ethanol, ethyl acetate, methanol, trifluoroethanol, methyl nonafluorobutyl, and deuterium oxide confirm the resolution of *J*-couplings, and the wideband capability for multinuclear NMR experiments. Table I compares with the state-of-the-art CMOS NMR sensing systems [1-5].

Acknowledgement

We thank program director Dr. Isik Kizilyalli of ARPA-E for the support of this research under contract DE-AR0001063.

References

[1] D. Krüger *et al*, *ESSCIRC*, 2022. [2] S. Hong, *et al*, *VLSI*, 2020. [3] S. Fan *et al*, *JSSC*, 2022. [4] K.-M. Lei *et al*, *An. Chem*, 2020. [5] K.-M. Lei *et al*, *ISSCC*, 2016.

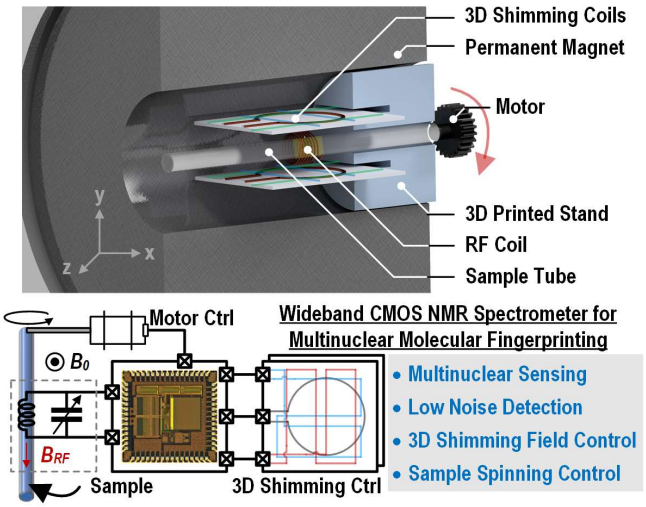

Fig. 1. Wideband CMOS multinuclear NMR spectrometer system.

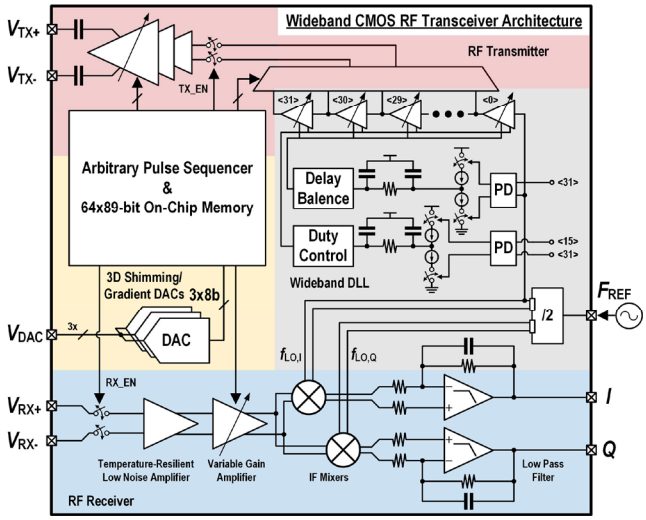

Fig. 2. Wideband CMOS RF transceiver architecture.

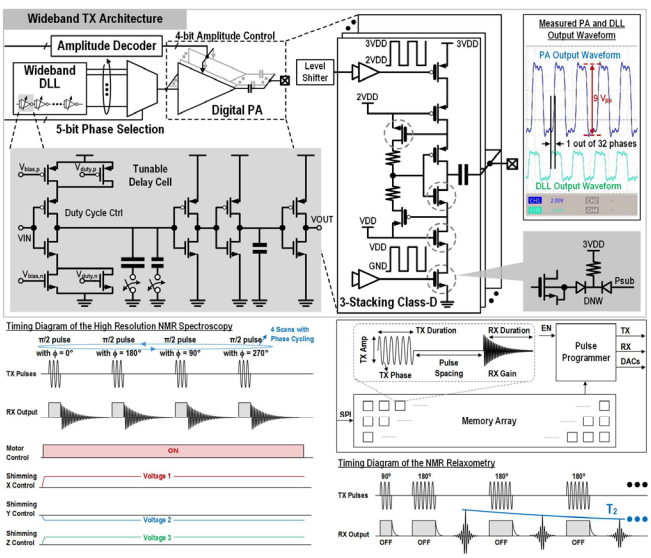

Fig. 3. Wideband TX architecture and NMR sequences.

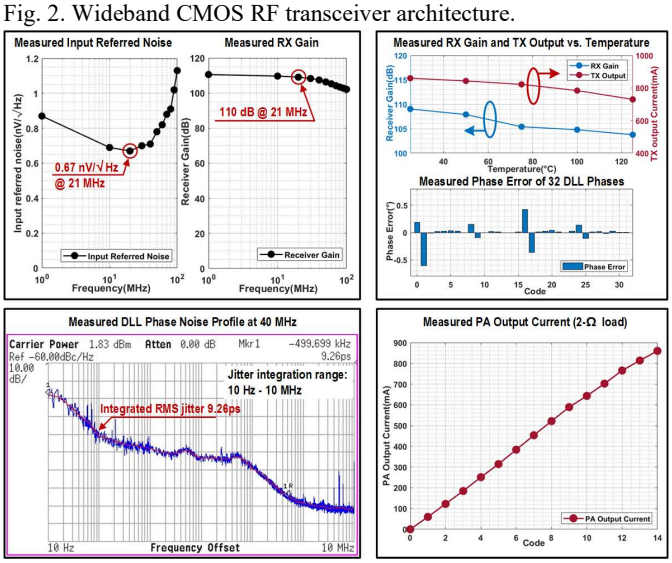

Fig. 4. Measured RX input referred noise and gain, DLL phase errors, temperature, phase noise and PA output current.

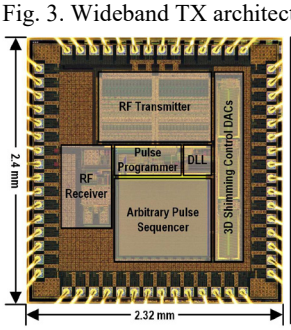

Fig. 5. Die Micrograph.

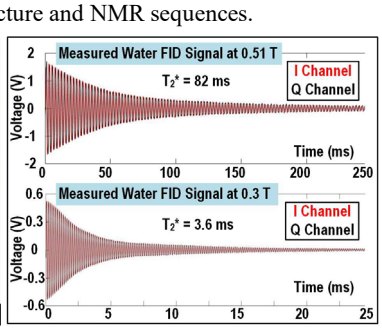

Fig. 6. Measured FID signals.

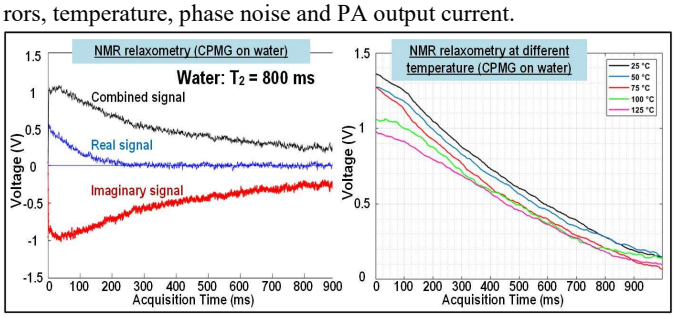

Fig. 7. Measured ^{1}H relaxation time T_2 at different temperatures.

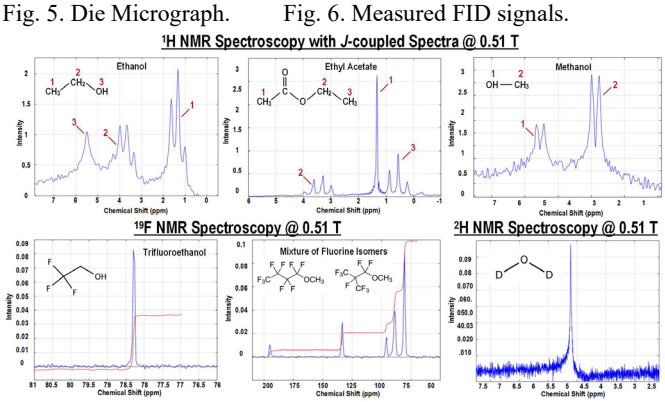

Fig. 8. Measured NMR ^{1}H spectroscopy with 0.07-ppm resolution and multinuclear NMR spectroscopy (^{1}H, ^{19}F, ^{2}H) results.

Table I. Comparison with state-of-the-art NMR spectrometers.

Specifications	This work	D. Krüger ESSCIRC'22	S. Fan JSSC'22	S. Hong VLSI'20	K Lei Analytical Chemistry'20	K. Lei ISSCC'16
System Performance						
Functionality	**NMR Relaxometry NMR Spectroscopy**	NMR Relaxometry NMR Spectroscopy	NMR Relaxometry	NMR Relaxometry	NMR Relaxometry NMR Spectroscopy	NMR Relaxometry
Magnet	**Permanent (0.3 T and 0.51 T)**	Permanent (0.51 T)	Permanent (0.52 T)	Permanent (0.5 T)	Permanent (0.51 T)	Permanent (0.46 T)
Shimming/ Gradient Control	**On-Chip**	On-Chip	Off-Chip	N/A	Off-Chip	N/A
Spectral Resolution	**0.07 ppm**	1 ppm	N/A	N/A	0.16 ppm	N/A
Multinuclear NMR	**Yes (^{1}H ^{19}F ^{2}H)**	No (^{1}H)	No (^{1}H)	No (^{1}H)	No (^{1}H)	No (^{1}H)
Circuit Performance						
Technology	**0.18μm CMOS**	0.18μm CMOS	0.18μm HV-CMOS SOI	0.18μm CMOS	0.18μm CMOS	0.18um CMOS
Frequency Range [MHz]	**1-100**	10-60	22.2	21	10-40	20
RX IRN [nV/√Hz]	**0.67**	0.78	0.63	0.95	0.82	1
RX Gain [dB]	**30-110**	30-100	85.2	65-125	34-100	87.6
TX Maximum Pout [mW]	**740**	220	602	84	182	16
TX Efficiency [%]	**49**	39	N/A	N/A	N/A	31.6
Area [mm²]	**5.6**	5	1.8	1.8	4	7.6